A Switchable High-Sensitivity Photodetecting and Photovoltaic Device with Perovskite Absorber

ARTICLE *in* JOURNAL OF PHYSICAL CHEMISTRY LETTERS · APRIL 2015

Impact Factor: 7.46 · DOI: 10.1021/acs.jpclett.5b00723

THE JOURNAL OF PHYSICAL CHEMISTRY Letters

Letter

pubs.acs.org/JPCL

A Switchable High-Sensitivity Photodetecting and Photovoltaic Device with Perovskite Absorber

Hsin-Wei Chen,[†,§] Nobuya Sakai,[‡] Ajay Kumar Jena,[†] Yoshitaka Sanehira,[†] Masashi Ikegami,[†] Kuo-Chuan Ho,[§] and Tsutomu Miyasaka*[,†]

[†]Graduate School of Engineering, Toin University of Yokohama, Kuroganecho 1614, Aoba, Yokohama, Kanagawa 225-8503, Japan

[‡]Department of Physics, University of Oxford, Parks Road, Oxford OX1 3PU, United Kingdom

[§]Department of Chemical Engineering, National Taiwan University, No. 1, Sec. 4, Roosevelt Road, Taipei 10617, Taiwan

Supporting Information

ABSTRACT: Amplified photocurrent gain has been obtained by photodiodes of inorganic semiconductors such as GaAs and Si. The avalanche photodiode, developed for high-sensitivity photodetectors, requires an expensive vapor-phase epitaxy manufacture process and high driving voltage (50−150 V). Here, we show that a low-cost solution-processed device using a planar-structured ferroelectric organo-lead triiodide perovskite enables light detection in a large dynamic range of incident power (10^{-7}−10^{-1} W cm^{-2}) by switching with small voltage (−0.9 to +0.5 V). The device achieves significantly high external quantum conversion efficiency (EQE) up to 2.4 × 10^5% (gain value of 2400) under weak monochromatic light. On a single dual-functional device, incident small power (0.2−100 μW cm^{-2}) and medium to large power (>0.1 mW cm^{-2}) are captured by reverse bias and forward bias modes, respectively, with linear responsivity of current. For weak light detection, the device works with a high responsivity value up to 620 A W^{-1}.

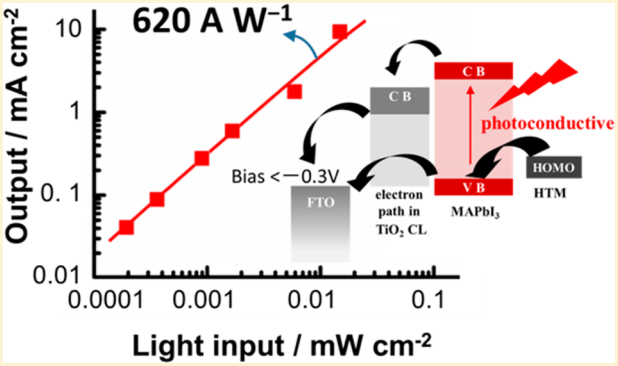

Large amplification of photoswitched current is mandatory for high-resolution image sensors[1] and photodetectors.[2] Amplified photocurrent in large excess of the theoretical limit of quantum efficiency (100%) is achieved by an avalanche photodiode made of inorganic semiconductors such as GaAs[3] and Si.[4] Such avalanche effect requires high quality crystals made by expensive vapor-phase epitaxy and high driving voltage (50−150 V) to cause ionization reaction. High-gain photodetectors are usually designed to maximize spectral responsivity of photocurrent under applied bias without combining the high function in photovoltaic power generation. Here, we show that a low-cost solution-processed device using a planar-structured film of organo-lead triiodide perovskite can electrically switch between a high-gain photodiode in reverse bias and a high-efficiency photovoltaic device in forward bias. Such dual-functional device enables high-sensitivity light detection in a large dynamic range of incident power (10^{-7}−10^{-1} W cm^{-2}) with small driving voltage (<1 V). We demonstrate that significant amplification of photodiode current occurs on a planar-structured ferroelectric perovskite film in junction with a bypass-rich TiO_2 blocking layer. The device generates amplified photodiode currents with significantly high external quantum conversion efficiency (EQE) up to 2.4 × 10^5% (gain value of 2400). Incident signals of small power density (0.2−100 μW cm^{-2}) and medium to large power density (>0.1 mW cm^{-2}) are captured on a single device by reverse bias and forward bias modes, respectively, with linear dependence of current. The dual-functional perovskite device can considerably expand the linear dynamic range of light detection and sensing.

Perovskite materials with crystal structure ABX_3 exhibit unique properties that find different interesting applications as electronic devices.[5] In perovskite, formation of dipoles due to structural transitions in the crystal lattice, from higher symmetry to lower symmetry, originates ferroelectric property, which is applied to condensers, transistors, and spintronic memories using metal oxide perovskites. These dipoles impart large dielectric constant and induce internal electric polarization, whose amplitude is regulated by the external electric field.[6] Thin films of ferroelectric perovskites can behave like a semiconducting diode under applied electric field that enhances dielectric constant.[7] Unlike $PbTiO_3$, $Pb(Zr,Ti)O_3$, and $BaTiO_3$,[7−12] which have large bandgaps and high electric resistance,[13] narrow bandgap perovskites such as $BiFeO_3$ generate a diode-like photocurrent at room temperature by visible light excitation.[6,14−18] Recently, Bi_2FeCrO_6 (bandgap, 1.4−1.6 eV) was found to function as an absorber of ferroelectric photovoltaic cell with efficiency as high as

Received: April 7, 2015
Accepted: April 23, 2015
Published: April 23, 2015

DOI: 10.1021/acs.jpclett.5b00723
J. Phys. Chem. Lett. 2015, 6, 1773−1779

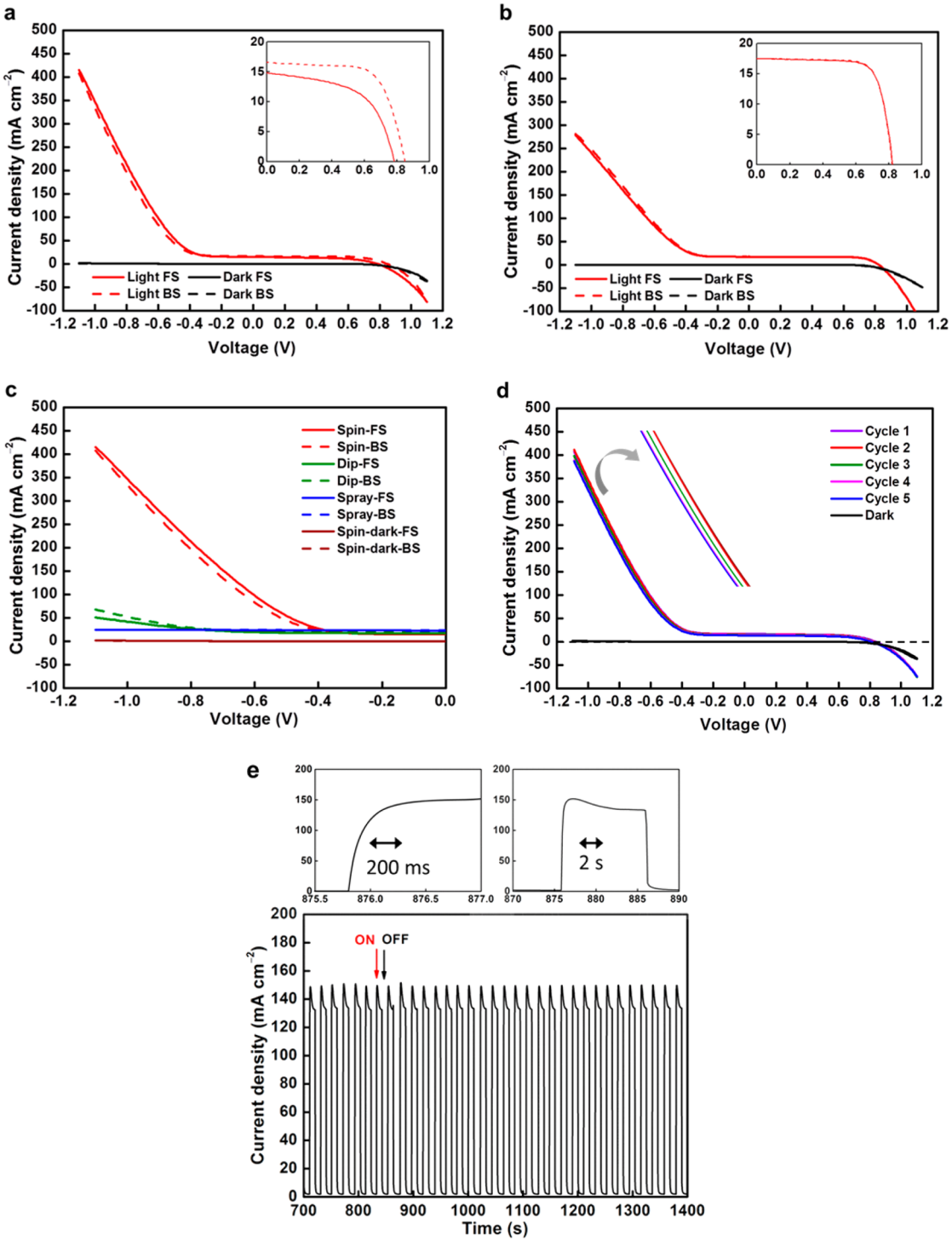

Figure 1. *J*−*V* curves with forward scan (FS) and backward scan (BS) for (a) planar structure and (b) meso-TiO_2 structure perovskite devices under exposure to white light (100 mW cm^{-2} = 1 sun) and in the dark. Insets are photovoltaic characteristics (enlarged) in the positive voltage range. (c) *J*−*V* curves (FS and BS) of amplified diode photocurrents in reverse bias for the planar structure devices with spin-coated, dip-coated, and spray-coated TiO_2 blocking CLs. (d) Repeated scan cycles of the *J*−*V* curve of amplified diode photocurrents for the planar device with spin-coated CL. (e) Time-dependent photocurrent response curves under repeated cycles of light switching on and off for planar devices under exposure to 1 sun. The response curve is an example of a pick up part from a continuous 200−1000 cycles.

3.3%.[19] Although these perovskites exhibit photoelectric response, their photoconductivity is not high enough to yield large current density. However, organo-lead halide perovskite emerged as a rare exception, which possesses high carrier mobility and photoconductivity. Since our first study of organo-lead halide-based solid-state photovoltaic cells in 2008[20] and 2009,[21] there has been a dramatic progress in power conversion efficiency toward 19−20%,[22,23] Such high efficiency has been achieved by a narrow bandgap perovskite, $CH_3NH_3PbI_3$ ($MAPbI_3$; bandgap, 1.55−1.6 eV).[21−23] $MAPbI_3$ exhibits ferroelectric property due to the organic cation in the hybrid structure.[24] With high dielectric constant >20,[25] $MAPbI_3$ is

DOI: 10.1021/acs.jpclett.5b00723
J. Phys. Chem. Lett. 2015, 6, 1773−1779

assumed to undergo polarization under external bias.[24] Similar to other ferroelectric perovskites $BiFeO_3$ and $Bi_{0.9}Sr_{0.1}FeO_{3-\delta}$,[26] $MAPbI_3$ is expected to work as a unique photodiode. Recently, high gain of diode photocurrent has been reported for $MAPbI_3$ either in photovoltaic devices[27] or photodiode devices.[28] Moehl et al. observed 150-fold amplification of short-circuit photocurrent (estimated gain value close to 150) with a mesoporous TiO_2-based perovskite photovoltaic device.[27] In contrast, Dong et al. reported much higher diode gain of 490 with a planar TiO_2-free perovskite device by maximizing photocurrent on sacrifice of photovoltaic output.[28] We have also reported the photocurrent amplification under reverse bias, which gives rise to transient ferroelectric polarization and hysteretic behavior of $MAPbI_3$ in photovoltaic cells,[29] where the largest hysteresis was found for a planar perovskite film. We report here that the planar $MAPbI_3$ prepared on a thin compact TiO_2 layer is capable of large avalanche-like amplification of diode photocurrent with diode gain up to 2400, while sustaining high photovoltaic performance. We also demonstrate that perovskite device exhibits robust stability in current amplification during repeated light switching on and off.

The perovskite-based devices were fabricated by solution coating processes under ambient air conditions as described previously.[29,30] A planar crystalline layer of $MAPbI_{3-x}Cl_x$ was formed on a thin compact TiO_2 hole-blocking layer (thickness, 50 nm) that passivates the surface of a conductive transparent F-doped SnO_2 (FTO) layer on glass substrate. As a reference, a mesoporous TiO_2 (meso-TiO_2) layer was employed as a scaffold of perovskite and formed on the above TiO_2 blocking layer. Spiro-MeOTAD (2,2(7,7(-tetrakis(*N*,*N*-di-*p*-methoxyphenylamine)9,9(-spirobifluorene))) containing dopants was coated on top of the $MAPbI_{3-x}Cl_x$ layer as a hole transporting material (HTM) and treated under dry air for further oxidative doping. Au was vacuum-deposited on the top as counter electrode. The thickness of the planar perovskite layer was around 300 nm, as shown in Supporting Information Figure S1. $MAPbI_{3-x}Cl_x$ was prepared by a Cl-added synthetic route according to the previous method.[22] Coating of the compact TiO_2, perovskite, and spiro-MeOTAD layers were conducted in ambient air by spin-coating methods with precursor solutions as described previously.[29,30] Here, the compact TiO_2 blocking layer (CL) plays a key role in regulating the diode performance of the device. Therefore, we employed three different types of CLs. High-density CL was prepared by gas-phase spray pyrolysis by spraying a $Ti(acac)_2(OC_3H_7)_2$ precursor in 2-propanol solution (0.19 M) on the FTO surface at 400 °C. In contrast, less compact CL was prepared by spin-coating method, in which the same precursor solution was spun on the FTO surface. In addition to the above two methods, a CL of medium compactness was prepared by repeated dip-coating method, in which the FTO substrate was dipped in $TiCl_4$ aqueous solution (20 mM) at 70 °C and sintered at 450 °C after drying. All these different CLs were made to have an average thickness of 50 nm.

Figure 1a shows the photocurrent density−voltage (*J*−*V*) characteristics obtained for a planar $MAPbI_{3-x}Cl_x$ device with a spin-coated TiO_2 layer. Here, external bias voltage was scanned forward (FS) and backward (BS) between −1.1 V and +1.1 V under white light irradiation (AM 1.5G simulated sunlight, 100 mW cm^{-2}). The inset is the photovoltaic *J*−*V* curve in which the device was applied forward (positive) bias voltage. Here, the positive sign of voltage (0 to 1.1 V) means that Au counter electrode is positive with respect to FTO. In the photovoltaic *J*−*V* curves, a hysteresis between FS and BS is most enhanced for the planar structure that is sensitive to ferroelectric polarization.[29] Figure 1b shows the result of the same measurement for a device of meso-TiO_2 structure. Both the devices yielded short-circuit current density (J_{SC}) of 15−18 mA cm^{-2} and open-circuit voltage (V_{OC}) exceeding 0.8 V with average power conversion efficiencies (PCEs) of 9.5−11% (Supporting Information Table S1). When the same device is switched to the photodiode mode by reverse bias, amplification of photocurrent started at voltage around −0.35 V. The energy level of this onset voltage coincides with the valence band level of perovskite, as discussed hereinafter. The current density dramatically increased and reached up to 410 mA cm^{-2} at −1.1 V. Theoretical fitting of initial current increase follows a characteristic of a conventional diode[6] (Supporting Information Figure S2). Current showed a linear increase beyond −0.6 V, indicating the appearance of Ohmic contact under high bias condition. In ferroelectric perovskites, Schottky barrier-to-Ohmic contacts transfer of the interfacial structures has been ascribed to flipping of vacancy species (oxygen in $BiFeO_3$[26]), which can correspond in the case of $MAPbI_3$ to diffusion of halogen and/or MA ions.[31] No current flowed at the same bias conditions in the dark. The EQE action spectrum of the giant amplified photocurrent (Figure 2) matches the optical absorption of perovskite. The magnitude of current density in ferroelectric materials is described as the product of polarization and conductivity.[16] Therefore, it is rationalized that the photoconductivity of perovskite enhances the gain of photocurrent, similar to commercial photodiodes. The maximum *J* value of the planar structure (410 mA cm^{-2}) was much larger than that generated by the meso-TiO_2 structure (270 mA cm^{-2}) (Figure 1b). This indicates that photoconductivity as well as the ferroelectricity of the planar bulk structure is larger than those of the meso-TiO_2 structures.

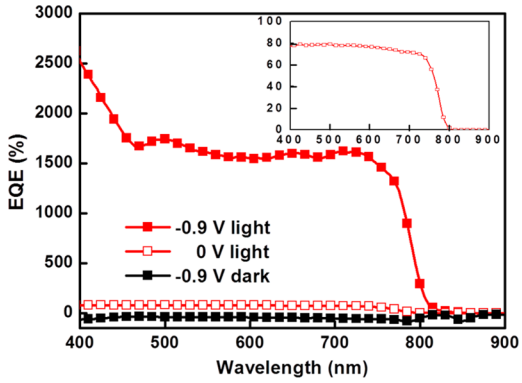

Figure 2. EQE action spectra for diode photocurrent and short-circuit current (J_{SC}) for a planar perovskite device (spin coat CL) biased at −0.9 and 0 V, respectively. Inset shows the action spectrum of J_{SC} (enlarged). The data was taken from a cell yielding conversion efficiency of 12.7% with J_{SC} of 17.8 mA cm^{-2} by BS. Incident power density used in this measurement was on the order of 1 mW cm^{-2}, the actual density depending on wavelength. The device was kept in the dark under open-circuit conditions prior to the measurement.

The photocurrent amplification in the reverse-bias mode was strongly controlled by the structure of the TiO_2 CL that rectifies current. Figure 1c shows the influence of the different CLs on the amplified photocurrent. The photocurrent amplification became largest for the planar perovskite on the spin-coated CL, while it is very small or absent for the same

DOI: 10.1021/acs.jpclett.5b00723
J. Phys. Chem. Lett. 2015, 6, 1773−1779

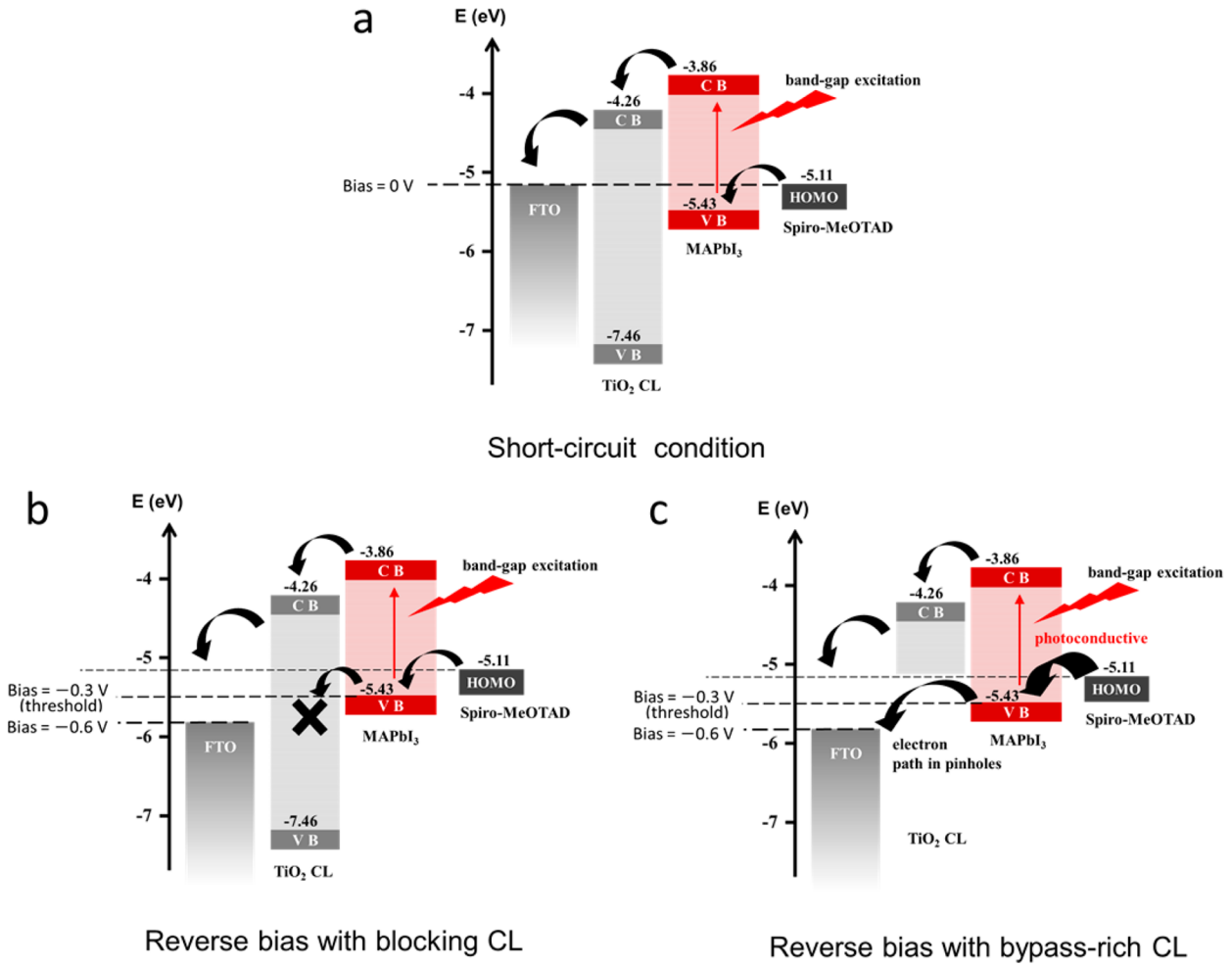

Figure 3. Energy diagrams and carrier transfer mechanism for amplified photodiode current generation. Band diagrams of (a) short-circuit condition ($V = 0$), (b) reverse bias condition ($V = -0.6$ V) with blocking TiO_2 CL (spray coat) that blocks charge transfer from VB, and (c) reverse bias ($V = -0.6$ V) with bypass-rich TiO_2 CL (spin coat), leading to generation of amplified current.

perovskite on the dip-coated CL and on the spray-coated CL. The origin of this discrepancy is the change of density/compactness of the CL. This fact was observed by the amplitude of leakage dark current in forward bias measured for different CLs, which was larger in the order of spin coat > dip coat > spray coat (Supplementary Figure S3). Apparently, spin-coated CL allows leakage current due to its poor compactness. The same conclusion has been reported by Moehl et al. for the porosity of TiO_2 that enhances current amplification.[27] The giant amplified current can flow with less compact TiO_2 CLs, while it is totally blocked by highly compact TiO_2 CL. Figure 1d exhibits repeatability of the amplified giant photocurrent on the planar $MAPbI_{3-x}Cl_x$/spin coat CL device. The photocurrent magnitude is quite stable and reproducible under repeated scans of $J-V$ curves. At a fixed bias voltage of −0.7 V, stable photocurrent (>150 mA cm^{-2}) is produced by repeated ON and OFF cycles under exposure to intense white light (100 mW cm^{-2}) up to 1000 times, as shown in Figure 1e.

Figure 2 exhibits the EQE action spectrum of the giant current for the planar device, measured at a bias of −0.9 V along with the reference EQE spectrum of J_{SC} under zero bias. The EQE value of the giant current reaches 1700% or more, while that of J_{SC} is around 80%. Flat spectral sensitivity with a sharp onset at 800 nm indicates that the origin of both J_{SC} and amplified current is band gap photoexcitation of $MAPbI_3$. In this EQE measurement, incident power of monochromatic light was on the order of 1 mW cm^{-2} at 550 nm. However, we observed significantly high and amplified EQE values that exceed 10^5% when light intensity is reduced down to 0.01 mW cm^{-2}. In other words, EQE values measured at high intensity of 1 mW cm^{-2}, corresponding to monochromatic portion of sunlight (100 mW cm^{-2}), is exhibiting a saturation in its light intensity dependence. More detailed analysis of this intensity-dependent characteristic will be described hereinafter.

Based on the results, the amplified photocurrent in reverse bias is explained as photoconductive current of $MAPbI_{3-x}Cl_x$ (substantially $MAPbI_3$), whose amplitude is strongly regulated by the TiO_2 CL. Figure 3 depicts the mechanism of current amplification. In short-circuit conditions (a), J_{SC} is rectified by electron injection to TiO_2. In forward (positive) bias, the device performs photovoltaic current generation, which is rectified in the same direction as the case of reverse bias (b) and (c). In the reverse bias conditions (b) and (c), electron transfer from the valence band (VB) of perovskite to the conductive electrode (FTO) can start at a threshold voltage of around −0.3 V. Here, because 0 V corresponds to the highest occupied molecular orbital (HOMO) level of spiro-MeOTAD, −0.3 V is located close to the VB of perovskite. The electron transfer to FTO is, however, blocked by the TiO_2 CL, which possesses a high conduction band (CB) and high resistance in the dark, as

DOI: 10.1021/acs.jpclett.5b00723
J. Phys. Chem. Lett. 2015, 6, 1773−1779

shown in (b). When this TiO_2 layer possesses a bypass of current flow by the formation of pinholes that are filled by photoconductive perovskite, VB electrons start flowing into FTO, as shown in the scheme of Figure 3c. Here, the gate of current flow opens when $MAPbI_3$ is excited to highly conductive state by visible light absorption. Photoconductivity of $MAPbI_3$ is considered to be responsible for diode photocurrent enhancement. Previous studies show that dipole polarization in $MAPbI_3$ is involved in conductivity increase under photoexcited state.[27,32] Further, ferroelectric and piezoelectric response have been found for planar $MAPbI_3$ films under external bias, which generates ferroelectricity-driven photocurrent.[33] Based on these facts and our previous work,[29] we consider that the planar structure perovskite permits large photoconductivity current under reverse bias as a result of ferroelectric dipole polarization that facilitates rectified photocurrent. In the photodiode structure studied here, bypass-rich CL allows the large amplified photocurrent, while the high-density CL that meets the situation of Figure 3b suppresses current amplification. We have also examined device structures in which either of CL or HTM is missing. They did not work as a normal photodetector because of large dark leakage current that accompanies the photocurrent. In addition, photocurrent was poorly rectified in the absence of carrier selective layers.

Light intensity dependence of the device current showed high sensitivity to light in a wide range of incident power. To choose sensitivity range, the device can be switched between photodiode mode and photovoltaic mode. Photodiode mode works with high responsivity for weak light detection backed by amplified current, while photovoltaic mode is more suitable for capture of intense light. In photovoltaic mode, photocurrent density remains stable at bias voltage from 0 to +0.5 V, and current response is very fast as generally found for perovskite-based photovoltaic cells (<1 μs[34]). Figure 4a shows the intensity dependence of photocurrent for a device biased at 0 V. Good linearity is held for intensity up to 100 mW cm^{-2} when the device was exposed to white sunlight. However, such linearity was not always obtained for giant current in reverse bias because high density current (0.2−0.4 A cm^{-2}) is mitigated by internal resistivity. Figure 4b shows intensity dependence measured for weak monochromatic light of 550 nm with incident power up to 10.3 mW cm^{-2}. For weak light detection, the device was switched to the photodiode mode biased at −0.7 V. Amplified photocurrent operated in photodiode mode (−0.7 V) greatly improves detectability. Photocurrent density dramatically increases by more than 2000 times larger than those obtained at 0 V. The diode current shows linear dynamic response to incident power density up to 0.1 mW cm^{-2}. Weak intensity monochromatic light, 0.2 μW cm^{-2}, was detected on the device by yielding 0.04 mA cm^{-2}. In photodiode property, an EQE value of 100% corresponds to a gain of 1. Dong et al. devised a high gain perovskite-based photodetector with a nonphotovoltaic structure to show photocurrent reaching a diode gain of 490 and responsivity values in terms of current output per incident power of 20−200 A W^{-1}.[28] Additionally, Yang et al. employed a PEDOT/perovskite/PCBM junction for a photodetector,[34] which showed high detectivity of light with intensity as small as 10^{-8} W cm^{-2}. However, the gain of photocurrent was the same level as J_{SC} without using the current amplification effect. In our device, based on the device characteristics of Figure 4b, responsivity value shows a level of 450 ± 150 A W^{-1} in the intensity range of 1 ∼ 50 μW cm^{-2}. The device exhibits the highest responsivity of 620 A W^{-1} at 10 μW cm^{-2} in the middle of linear region. Here, we also found that the gain of current output in the weak light detection is significantly high. Photocurrent density at 0 V (J_{SC}) gives a standard EQE value of around 80% (see Figure 2, inset) that corresponds to a gain of 0.8. Therefore, the gain of photodiode current (−0.7 V) is obtained on the basis of the ratio of current densities at −0.7 and 0 V in Figure 4b. For small incident power in a range of 2 to 20 μW cm^{-2}, the gain value reached 2400 ± 100. These values largely exceed the highest gain ever achieved by perovskite-based photodetectors.[27,28,34] The response speed of amplified photocurrent depended on the bias voltage; a device biased at −0.7 V showed a slow response with saturation time 100−200 ms (Supporting Information Figure S4). In Figure 4b, the responsivity of the diode current tends to deviate from linearity at high monochromatic intensity over 0.1 mW cm^{-2}. In the intensity range of 0.1−0.3 mW cm^{-2}, which corresponds to a measured current density of 50−150 mA cm^{-2}, the current starts to saturate, and the gain values decrease to 500 ± 50. For this behavior, we assume that the series resistance of our device (∼10 Ω) is controlling the maximum current in the linear dynamic range of responsivity. On the perovskite-based photodetective and photovoltaic device, the diode-mode operation enables avalanche-like high gain detection of weak light, and the photovoltaic operation guarantees high responsivity to intense light.

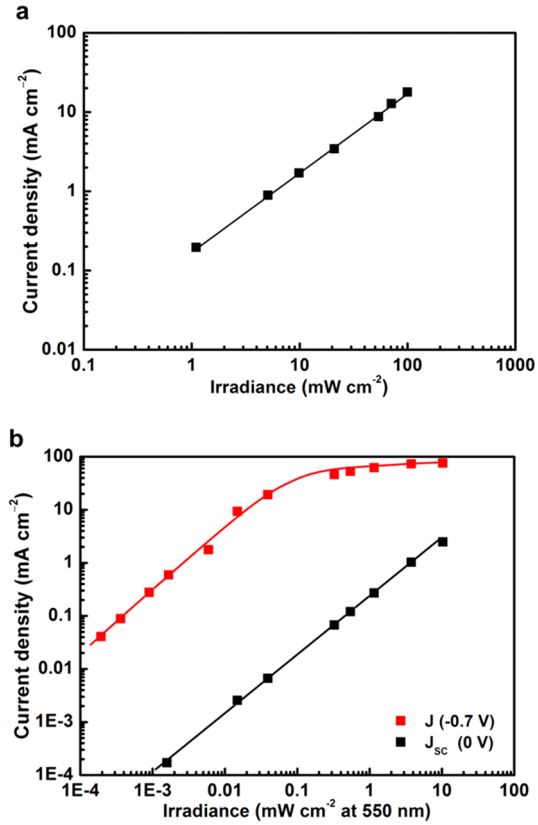

Figure 4. Light intensity-dependent characteristics of photocurrent density for a planar perovskite device with a spin-coated blocking layer. (a) Linear dependence of J_{SC} (biased at 0 V) on intense sunlight (AM 1.5). (b) Dynamic range in intensity dependence of perovskite photodiode current for monochromatic light of 550 nm. Device was biased at 0 V (corresponding to J_{SC}) and −0.7 V (amplified diode current mode). All measurements were conducted at room temperature in ambient air. Devices were kept in the dark under open-circuit conditions prior to the measurement.

DOI: 10.1021/acs.jpclett.5b00723
J. Phys. Chem. Lett. 2015, 6, 1773−1779

In this study, a large and linear dynamic range of light detection/sensing was realized by incorporating photodiodes and photovoltaic functions into a single device structure bearing the planar ferroelectric perovskite film as an absorber. We demonstrated that the performance of the perovskite-based optoelectronic device can compete with avalanche photodiodes with the advantages of low-cost solution process, low voltage of device operation, and wide dynamic range of linear light detection backed by dual-functional responsivity. In addition, the tunable spectral sensitivity of the device is the fundamental merit of the organo-lead trihalide perovskite materials whose absorption wavelengths are changed by replacing the halogen anion. Further study on ferroelectric photoconductivity, dielectric polarization, and charge accumulation in the organo-lead halide perovskites will lead to discovery of new applications of the perovskite-based optoelectronic device.

■ ASSOCIATED CONTENT

Supporting Information

Experimental methods, scanning electron microscope (SEM) images, exponential fit for $J-V$ curves, time-dependent photocurrent response curves, and table of photovoltaic characteristics are included in the Supporting Information. The Supporting Information is available free of charge on the ACS Publications website at DOI: 10.1021/acs.jpclett.5b00723.

■ AUTHOR INFORMATION

Corresponding Author

*E-mail: miyasaka@toin.ac.jp; Tel: +86-45-974-5055.

Notes

The authors declare no competing financial interest.

■ ACKNOWLEDGMENTS

This research is supported by the Japan Science and Technology Agency (JST) Advanced Low Carbon Technology R&D program (ALCA). T.M. acknowledges the support from the Japanese Society for Promotion of Science (JSPS) Grant-in-Aid for Scientific Research B. H.W.C. thanks E. Sakanoshita for her assistance in device fabrication and measurements.

■ REFERENCES

(1) Goda, K.; Tsia, K. K.; Jalali, B. Serial Time-Encoded Amplified Imaging for Real-Time Observation of Fast Dynamic Phenomena. *Nature* **2009**, *458*, 1145−1149.

(2) Hudelist, F.; Kong, J.; Liu, C.; Jing, J.; Ou, Z. Y.; Zhang, W. Quantum Metrology with Parametric Amplifier-Based Photon Correlation Interferometers. *Nat. Commun.* **2014**, *5*, 3049.

(3) Zhou, P. Y.; Dou, X. M.; Wu, X. F.; Ding, K.; Li, M. F.; Ni, H. Q.; Niu, Z. C.; Jiang, D. S.; Sun, B. Q. Single-Photon Property Characterization of 1.3 μm Emissions from InAs/GaAs Quantum Dots Using Silicon Avalanche Photodiodes. *Sci. Rep.* **2014**, *4*, 3633.

(4) Thomas, O.; Yuan, Z. L.; Shields, A. J. Practical Photon Number Detection with Electric Field-Modulated Silicon Avalanche Photodiodes. *Nat. Commun.* **2014**, *3*, 644.

(5) Mitzi, D. B. Synthesis, Structure, and Properties of Organic-Inorganic Perovskites and Related Materials. In *Progress in Inorganic Chemistry*; John Wiley & Sons, Inc.: New York, 2007; Vol. *48*, pp 1−121.

(6) Choi, T.; Lee, S.; Choi, Y. J.; Kiryukhin, V.; Cheong, S. W. Switchable Ferroelectric Diode and Photovoltaic Effect in $BiFeO_3$. *Science* **2009**, *324*, 63−66.

(7) Blom, P. W. M.; Wolf, R. M.; Cillessen, J. F. M.; Krijn, M. P. C. M. Ferroelectric Schottky Diode. *Phys. Rev. Lett.* **1994**, *73*, 2107−2110.

(8) Pintilie, L.; Vrejoiu, I.; Hesse, D.; LeRhun, G.; Alexe, M. Ferroelectric Polarization-Leakage Current Relation in High Quality Epitaxial Pb(Zr, Ti)O_3 Films. *PhRvB* **2007**, *75*, 104103.

(9) Pan, R. K.; Zhang, T. J.; Wang, J. Z.; Ma, Z. J.; Wang, J. Y.; Wang, D. F. Rectifying Behavior and Transport Mechanisms of Currents in Pt/$BaTiO_3$/Nb:$SrTiO_3$ Structure. *J. Alloys Compd.* **2012**, *519*, 140−143.

(10) Chen, Z.; He, L.; Zhang, F.; Jiang, J.; Meng, J.; Zhao, B.; Jiang, A. The Conduction Mechanism of Large On/Off Ferroelectric Diode Currents in Epitaxial (111) $BiFeO_3$ Thin Film. *J. Appl. Phys.* **2013**, *113*, 184106.

(11) Zhao, P.; Bian, L.; Wang, L.; Xu, J.; Chang, A. Enhanced Open Voltage of $BiFeO_3$ Polycrystalline Film by Surface Modification of Organolead Halide Perovskite. *Appl. Phys. Lett.* **2014**, *105*, 013901.

(12) Yang, S. Y.; Martin, L. W.; Byrnes, S. J.; Conry, T. E.; Basu, S. R.; Paran, D.; Reichertz, L.; Ihlefeld, J.; Adamo, C.; Melville, A.; et al. Photovoltaic Effects in $BiFeO_3$. *Appl. Phys. Lett.* **2009**, *95*, 062909.

(13) Dawber, M.; Rabe, K. M.; Scott, J. F. Physics of Thin-Film Ferroelectric Oxides. *Rev. Mod. Phys.* **2005**, *77*, 1083−1130.

(14) Basu, S. R.; Martin, L. W.; Chu, Y. H.; Gajek, M.; Ramesh, R.; Rai, R. C.; Xu, X.; Musfeldt, J. L. Photoconductivity in $BiFeO_3$ Thin Films. *Appl. Phys. Lett.* **2008**, *92*, 091905.

(15) Hauser, A. J.; Zhang, J.; Mier, L.; Ricciardo, R. A.; Woodward, P. M.; Gustafson, T. L.; Brillson, L. J.; Yang, F. Y. Characterization of Electronic Structure and Defect States of Thin Epitaxial $BiFeO_3$ Films by UV−Visible Absorption and Cathodoluminescence Spectroscopies. *Appl. Phys. Lett.* **2008**, *92*, 222901.

(16) Maksymovych, P.; Jesse, S.; Yu, P.; Ramesh, R.; Baddorf, A. P.; Kalinin, S. V. Polarization Control of Electron Tunneling into Ferroelectric Surfaces. *Science* **2009**, *324*, 1421−1425.

(17) Lee, D.; Baek, S. H.; Kim, T. H.; Yoon, J. G.; Folkman, C. M.; Eom, C. B.; Noh, T. W. Polarity Control of Carrier Injection at Ferroelectric/Metal Interfaces for Electrically Switchable Diode and Photovoltaic Effects. *Phys. Rev. B* **2011**, *84*, 125305.

(18) Kim, T. H.; Jeon, B. C.; Min, T.; Yang, S. M.; Lee, D.; Kim, Y. S.; Baek, S. H.; Saenrang, W.; Eom, C. B.; Song, T. K.; et al. Continuous Control of Charge Transport in Bi-deficient $BiFeO_3$ Films through Local Ferroelectric Switching. *Adv. Funct. Mater.* **2012**, *22*, 4962−4968.

(19) Nechache, R.; Harnagea, C.; Li, S.; Cardenas, L.; Huang, W.; Chakrabartty, J.; Rosei, F. Bandgap Tuning of Multiferroic Oxide Solar Cells. *Nat. Photonics* **2015**, *9*, 61−67.

(20) Kojima, A.; Teshima, K.; Shirai, Y.; Miyasaka, T. Novel Photoelectrochemical Cell with Mesoscopic Electrodes Sensitized by Lead-Halide Compounds (11). Presented at the 214th ECS Meeting, Abstract #27, Honolulu, Hawaii, October, 2008.

(21) Kojima, A.; Teshima, K.; Shirai, Y.; Miyasaka, T. Organometal Halide Perovskites as Visible-Light Sensitizers for Photovoltaic Cells. *J. Am. Chem. Soc.* **2009**, *131*, 6050−6051.

(22) Lee, M. M.; Teuscher, J.; Miyasaka, T.; Murakami, T. N.; Snaith, H. J. Efficient Hybrid Solar Cells Based on Meso-superstructured Organometal Halide Perovskites. *Science* **2012**, *338*, 643−647.

(23) Zhou, H.; Chen, Q.; Li, G.; Luo, S.; Song, T. B.; Duan, H. S.; Hong, Z.; You, J.; Liu, Y.; Yang, Y. Interface Engineering of Highly Efficient Perovskite Solar Cells. *Science* **2014**, *345*, 542−546.

(24) Stoumpos, C. C.; Malliakas, C. D.; Kanatzidis, M. G. Semiconducting Tin and Lead Iodide Perovskites with Organic Cations: Phase Transitions, High Mobilities, and near-Infrared Photoluminescent Properties. *Inorg. Chem.* **2013**, *52*, 9019−9038.

(25) Brivio, F.; Butler, K. T.; Walsh, A.; van Schilfgaarde, M. Relativistic Quasiparticle Self-Consistent Electronic Structure of Hybrid Halide Perovskite Photovoltaic Absorbers. *Phys. Rev. B* **2014**, *89*, 155204.

(26) Guo, Y.; Guo, B.; Dong, W.; Li, H.; Liu, H. Evidence for Oxygen Vacancy or Ferroelectric Polarization Induced Switchable Diode and Photovoltaic Effects in $BiFeO_3$ Based Thin Films. *Nanotechnology* **2013**, *24*, 275201.

(27) Moehl, T.; Im, J. H.; Lee, Y. H.; Domanski, K.; Giordano, F.; Zakeeruddin, S. M.; Dar, M. I.; Heiniger, L. P.; Nazeeruddin, M. K.;

DOI: 10.1021/acs.jpclett.5b00723
J. Phys. Chem. Lett. 2015, 6, 1773−1779

Park, N. G.; et al. Strong Photocurrent Amplification in Perovskite Solar Cells with a Porous TiO_2 Blocking Layer under Reverse Bias. *J. Phys. Chem. Lett.* **2014**, *5*, 3931−3936.
(28) Dong, R.; Fang, Y.; Chae, J.; Dai, J.; Xiao, Z.; Dong, Q.; Yuan, Y.; Centrone, A.; Zeng, X. C.; Huang, J. High-Gain and Low-Driving-Voltage Photodetectors Based on Organolead Triiodide Perovskites. *Adv. Mater.* **2015**, *27*, 1912−1918.
(29) Chen, H. W.; Sakai, N.; Ikegami, M.; Miyasaka, T. Emergence of Hysteresis and Transient Ferroelectric Response in Organo-Lead Halide Perovskite Solar Cells. *J. Phys. Chem. Lett.* **2015**, *6*, 164−169.
(30) Kim, H. S.; Lee, C. R.; Im, J. H.; Lee, K. B.; Moehl, T.; Marchioro, A.; Moon, S. J.; Humphry-Baker, R.; Yum, J. H.; Moser, J. E.; et al. Lead Iodide Perovskite Sensitized All-Solid-State Submicron Thin Film Mesoscopic Solar Cell with Efficiency Exceeding 9%. *Sci. Rep.* **2012**, *2*, 591.
(31) Xiao, Z.; Yuan, Y.; Shao, Y.; Wang, Q.; Dong, Q.; Bi, C.; Sharma, P.; Gruverman, A.; Huang, J. Giant Switchable Photovoltaic Effect in Organometal Trihalide Perovskite Devices. *Nat. Mater.* **2014**, *14*, 193−198.
(32) Gottesman, R.; Haltzi, E.; Gouda, L.; Tirosh, S.; Bouhadana, Y.; Zaban, A. Extremely Slow Photoconductivity Response of $CH_3NH_3PbI_3$ Perovskites Suggesting Structural Changes under Working Conditions. *J. Phys. Chem. Lett.* **2014**, *5*, 2662−2669.
(33) Chen, B.; Shi, J.; Zheng, X.; Zhou, Y.; Zhu, K.; Priya, S. Ferroelectric Solar Cells Based on Inorganic−Organic Hybrid Perovskites. *J. Mater. Chem. A* **2015**, *3*, 7699−7705.
(34) Dou, L.; Yang, Y. M.; You, J.; Hong, Z.; Chang, W. H.; Li, G.; Yang, Y. Solution-Processed Hybrid Tperovskite Photodetectors with High Detectivity. *Nat. Commun.* **2014**, *5*, 5404.

DOI: 10.1021/acs.jpclett.5b00723
J. Phys. Chem. Lett. 2015, 6, 1773−1779